# Understanding the Metal-Directed Growth of Single-Crystal M-TCNQF₄ Organic Nanowires with Time-Resolved, in Situ X-ray Diffraction and First-Principles Theoretical Studies

Kai Xiao,*,[†] Mina Yoon,[†,‡] Adam J. Rondinone,[†] Edward A. Payzant,[†] and David B. Geohegan*,[†]

[†]Center for Nanophase Materials Sciences, and [‡]Materials Science and Technology Division, Oak Ridge National Laboratory, Oak Ridge, Tennessee 37831, United States

Ⓢ Supporting Information

ABSTRACT: The deterministic growth of oriented crystalline organic nanowires (CONs) from the vapor−solid chemical reaction (VSCR) between small-molecule reactants and metal nanoparticles has been demonstrated in several studies to date; however, the growth mechanism has not yet been conclusively understood. Here, the VSCR growth of M-TCNQF₄ (where M is Cu- or Ag-) nanowires is investigated both experimentally and theoretically with time-resolved, in situ X-ray diffraction

(XRD) and first-principles atomistic calculations, respectively, to understand how metals (M) direct the assembly of small molecules into CONs, and what determines the selectivity of a metal for an organic vapor reactant in the growth process. Analysis of the real-time growth kinetics data using a modified Avrami model indicates that the formation of CONs from VSCR follows a one-dimensional ion diffusion-controlled tip growth mechanism wherein metal ions diffuse from a metal film through the nanowire to its tip where they react with small molecules to continue growth. The experimental data and theoretical calculations indicate that the selectivity of different metals to induce nanowire growth depends strongly upon effective charge transfer between the organic molecules and the metal. Specifically, the experimental finding that Cu ions can exchange and replace Ag ions in Ag-TCNQF₄ to form Cu-TCNQF₄ nanowires is explained by the significantly stronger chemical bond between Cu and TCNQF₄ molecules than for Ag, due to the strong electronic contribution of Cu d-orbitals near the Fermi level. Understanding how to control the VSCR growth process may enable the synthesis of novel organic nanowires with axial or coaxial p/n junctions for organic nanoelectronics and solar energy harvesting.
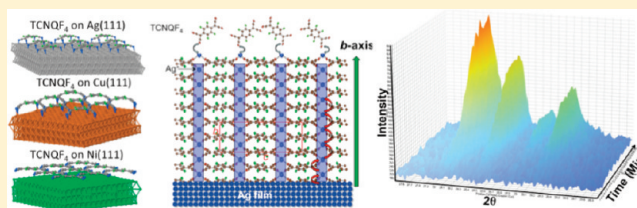
INTRODUCTION

Crystalline organic nanowires (CONs) assembled from semi-conducting small molecules offer a new and promising building block for highly efficient organic photovoltaics (OPVs).[1−3] The crystalline structure of CONs is innately advantageous compared to the morphological disorder (and low charge mobility) of polymers,[4] and their one-dimensional (1D) microscale morphology promises a pathway to overcome the anisotropic transport limitations of small-molecule thin films to achieve the high mobilities and directional transport required for OPVs and organic field-effect transistors (OFETs).[5−7] Because small molecules self-assemble through strong π−π interactions along the long axis of CONs, one-dimensional structure of CONs is promising to increase charge separation and exciton migration. CONs that would include alternating p- and n-type organic semiconductors in axial or coaxial geometries offer many potential advantages to develop more efficient OPV devices, including longer exciton diffusion lengths, very high surface-area p/n interfaces for exciton dissociation, and the possibility of three-dimensional nanoscale architectures.[8] Vertically aligned nanowire architectures have been found advantageous for OPVs,[5] whereas parallel-aligned nanowires on dielectric surfaces have been successfully employed to build OFETs.[6] Nevertheless, there are still

numerous challenges to overcome for the future fabrication of organic nanowire-based devices, including the development of synthesis and processing methods that can simultaneously grow nanostructures with well-defined positions, orientations, and controllable structures.

For the past few years, our research group and others have been working on an alternative strategy to integrate the growth and assembly of organic nanowires (NWs) using a VSCR method.[9−12] The defining characteristic of this approach is to utilize a metal region to simultaneously localize and direct the growth by providing part of the reactants necessary to sustain the chemical reaction. As the metal atoms from a metal film or nanoparticle react with the organic molecules, they become directly incorporated into the organic crystal between layers of organic molecules that tend to assemble in the π−π stacking direction. Systematic synthesis studies have shown that the size, structure, orientation, and position of the organic NWs can be controlled by spatially confining the chemical reactions and directional growth processes.[6,13,14] This growth process addresses the challenge of controlling the growth, orientation, and position of organic NWs that are typically synthesized
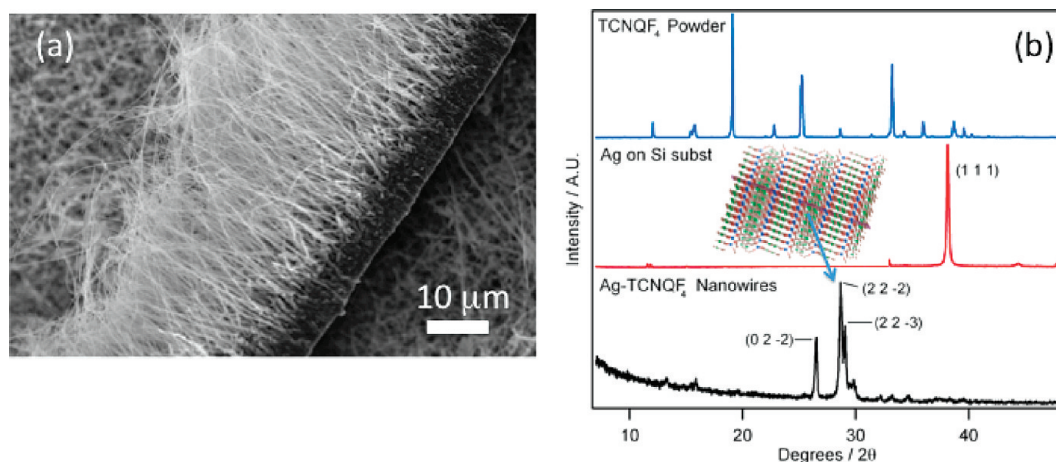
Figure 1. (a) SEM images of Ag-TCNQF$_4$ NWs. The array of NWs is separated from the substrate by an underlying Ag-TCNQF$_4$ layer. (b) The XRD patterns of TCNQF$_4$ powder, as-deposited Ag film, and as-grown Ag-TCNQF$_4$ NWs. Inset shows the crystalline structure and $(22\bar{2})$ crystalline face of the nanowires.

without catalyst assistance from the self-assembly of molecules,[15,16] unlike the deterministic growth of inorganic NWs.[17] Vertical or horizontal patterns of organic NWs have been achieved by the VSCR method through the defined placement of metals using optical lithography.[18,19] These concepts have been applied to grow organic NWs directly between electrodes to form FETs and memory devices.[20,21] However, despite this progress, the mechanisms of nanowire nucleation and the processes that define CON growth kinetics in the VSCR method are not well understood. How metals direct small molecules to assemble into CONs and the factors determining the selectivity of a metal for an organic vapor reactant remain open questions in the selective and deterministic growth of CONs by VSCR. A more profound understanding of these growth mechanisms is still required in order to enable the precise control of the morphological and functional properties of crystalline organic NWs.

Time-resolved in situ XRD is a powerful technique to probe the structure evolution of crystalline and nanoscale materials under controlled environmental conditions.[22–24] The relatively deep penetration depth of X-rays in soft organic matrices permits X-ray diffraction's use as a real-time probe of the overall crystallinity of an ensemble of organic NWs during growth. Therefore, in situ time-resolved XRD has a great potential to help elucidate the interfacial kinetics of restricted diffusion and the surface-specific reactions in the growth of CONs by the VSCR method.

In this paper, time-resolved in situ XRD is used to measure the nucleation and growth kinetics of M-TCNQF$_4$ NWs (M = Cu, Ag) in order to understand how metals direct the assembly of small-molecules into NWs and the factors governing the selectivity of a metal for an organic vapor reactant in the deterministic VSCR growth process. The growth kinetics of highly crystalline Ag- and Cu-TCNQF$_4$ NWs were explored under a range of temperature conditions. An analysis of the growth kinetics with a modified Avrami model indicates that the VSCR formation of NWs corresponds to 1D ion-diffusion-controlled tip growth. The kinetics imply that metal ions migrate from the metal film at the base of a NW, and diffuse through the NW to the tip, where they react with small molecules to propagate the growth of the NW. First-principles atomistic modeling is presented which give new insight into the initial interaction between different metals and TCNQF$_4$, the

interaction between the M-TCNQF$_4$ reaction product and the metal film, and the diffusion of metal atoms through metal films and M-TCNQF$_4$ NWs. Our theoretical study demonstrates the importance of such interactions in stabilizing the structure of the NWs and supports many aspects of the experimental observations. Understanding this growth process and mechanism could open up a promising avenue to synthesize organic single-crystal nanomaterials and metal−organic frameworks (MOFs) for organic nanoscale devices.

■ EXPERIMENTAL METHODS

Time-resolved, in situ XRD was used to investigate NW synthesis and metal disappearance during the VSCR growth process. The HT-XRD system consists of a PANalytical X'Pert Pro MPD θ/θ X-ray diffractometer equipped with an Anton Paar XRK-900 furnace and an X'Celerator solid-state detector. The metal film was deposited on a Si substrate in an e-beam deposition system. TCNQF$_4$ powder was placed in wells on the HT-XRD sample holder adjacent to the metal film. The reaction cell allows N$_2$ gas switching near the sample. Diffraction images were accumulated using an X'Celerator solid-state detector during the NW growth under N$_2$ gas flow at different temperatures. The growth of Ag-TCNQF$_4$ nanowires was thermally promoted by a temperature ramp experiment at around 10 °C/min under in situ XRD observation to investigate the nanowire evolution and to establish a suitable isothermal reaction temperature range. As shown in Supporting Information Figure S1, The $(22\bar{2})$ diffraction peak of Ag-TCNQF$_4$ begins to be detected at a temperature of ~160 °C and the growth is almost complete at 230 °C as evidenced by the lack of detection of Ag(111) diffraction peak, resulting from the complete consumption of the Ag film. Additional growth kinetics were measured for fixed growth temperatures at 160, 170, 180, 190 °C to determine kinetic parameters in the growth process.

Computational Methodology. We employed a highly accurate, all-electron first-principles quantum mechanical calculation code with numerical atom-centered orbitals (NAO) as basis set (FHI-aims);[25] the standard "tight" basis set was used. We used exchange-correlation functionals approximated within the local-density approximation (LDA)[26,27] and generalized gradient approximations (GGA) using a Perdew−Burke−Ernzerhof (PBE) functional,[28,29] including spin-polarization and relativistic effects.[25] All the molecular structures were fully relaxed for a given functional using the Broyden−Fletcher−Goldfarb−Shanno relaxation scheme,[30] with the maximum residual force on each atom less than 0.02 eV/Å. In a combination of these calculation settings, k-point sampling with 25 × 25 × 25 points in x,y,z directions was sufficient to converge the lattice parameters of the fcc bulk phase, the lattice parameter of Ag is 4.15 Å for PBE (4.01 Å for

14354

dx.doi.org/10.1021/ja301456p | *J. Am. Chem. Soc.* 2012, 134, 14353−14361
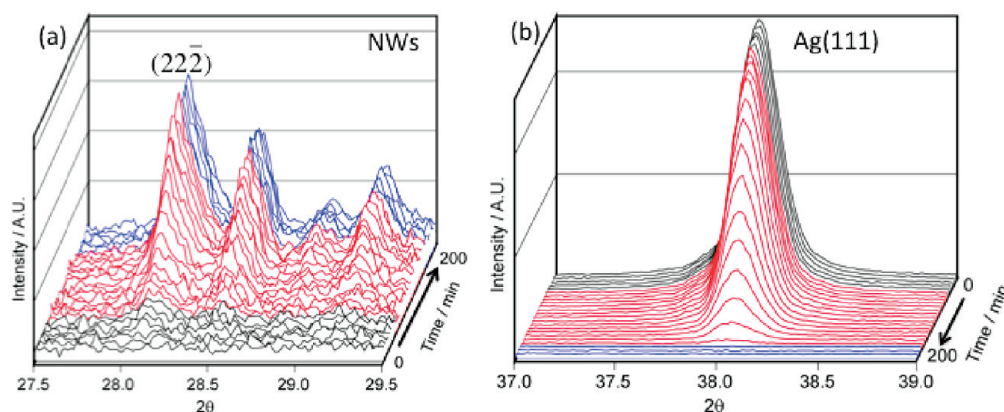
Figure 2. Time-resolved in situ XRD patterns for synthesis of Ag-TCNQF$_4$ NWs by vapor-solid reaction methods at 170 °C. (a) The ($22\bar{2}$) reflection of Ag-TCNQF$_4$ NWs corresponding with the time; (b) the Ag(111) reflection with the time. The black curves indicate that the Ag-TCNQF$_4$ NWs are not produced yet; the red curves indicate that the Ag-TCNQF$_4$ NWs are growing, while the Ag film is being consumed because of the reaction with the TCNQF$_4$ vapor; the blue curves indicate that the NW growth is completed due to complete consumption of the Ag film was consumed.

LDA, 4.09 Å for experiment), Cu is 3.67 Å for PBE (3.55 Å for LDA, 3.61 Å for experiment), and Ni is 3.50 Å for PBE (3.95 Å for LDA, 3.52 Å for experiment). In summary, all the lattice parameters from PBE results are in excellent agreement with experimentally measured values: differing only by 1.47% for Ag, 1.66% for Cu, and 0.57% for Ni.

We constructed a supercell consisting of TCNQF$_4$ molecules on 4 monolayers (ML) of 5 × 5 (111) metal (M = Ag, Cu, and Ni) films, with a large-size vacuum of 50 Å to ensure converged results. Our calculations were also compared from the pseudopotentials and plane-wave calculations using the Vienna Ab-initio Simulation Package (VASP)[31] and the PBE functional.[28,29] The energy cutoff for the plane-wave basis set was 400 eV and Monkhorst−Pack k-point sampling[32] with 3 × 3 × 1 k-points was used.

We considered Ag/Cu films and Ni/Cu films consisting of a total of 12 ML (6 ML for each metals) with fcc (111) 5 × 5 surfaces. Figure 6 shows the configuration, with brown balls, gray balls, and green balls for Cu, Ag, and Ni atoms, respectively. Each layer (L) is labeled from L1 to L6, where L1s are the interface (I) layers and L6s are the surface (S) layers. We substitutionally doped Cu films by Ni atoms and Ni films by Cu atoms and calculated changes in total energies with respect to the nondoped structures. Similar calculations were performed for Ag and Cu. In this case, the system consists of 300 atoms and we employed Sutton−Chen many-body force field approach[33−35] to effectively calculate total energies of a large system. This approach has been known to describe cohesive properties of fcc transition metals, such as Cu, Ag, and Ni, very well.

■ RESULTS AND DISCUSSION

The growth kinetics of organic NWs were probed during the reaction and growth of TCNQF$_4$ vapor with metal (Ag or Cu) film on the Si substrate at multiple temperatures. The resulting Ag-TCNQF$_4$ NWs were characterized by scanning electron microscopy (SEM) as shown in Figure 1a. It is worth noting that the array of NWs is separated from the substrate by an underlying Ag-TCNQF$_4$ layer, the importance of which in understanding the detailed growth mechanism will be discussed below. Moreover, the formation of such an underlying film is of particular relevance for ordered bulk heterojunction OPVs since it might be highly beneficial as exciton and electron (hole) blocking layer.[36] The crystalline phases corresponding to the TCNQF$_4$ powder, the Ag film on the Si substrate, and the as-grown Ag-TCNQF$_4$ NWs were easily identified by XRD,[18,37] as shown in Figure 1b. The (111) peak of Ag at $2\theta = 38°$ and ($22\bar{2}$) peak of Ag-TCNQF$_4$ NWs at $2\theta = 28°$ were selected as the signature peaks to track the kinetics of the NW growth and

the evolution of the metal because of their high intensity and because the ($22\bar{2}$) crystalline face of the NWs is parallel to the benzene ring in the crystal structure that corresponds to the $\pi-\pi$ stacking face along the growth direction.

To understand the onset temperature for Ag-TCNQF$_4$ NW growth and establish a suitable isothermal reaction temperature range, a temperature ramp experiment under in situ XRD observation was performed. The onset of formation of Ag-TCNQF$_4$ occurs at approximately 160 °C (Supporting Information Figure S1). We did not observe any phase transition or new phase produced in the growth. Isothermal growth experiments were then performed at 160, 170, 180, and 190 °C while real-time XRD recorded the kinetics of the growth process. Figure 2 displays the time-resolved XRD data collected for Ag-TCNQF$_4$ NW growth at 170 °C. Ranges of 27−30° and 37−39° were chosen for the real-time 2θ scans during the growth experiments because they capture the preselected Ag-TCNQF$_4$ ($22\bar{2}$) and Ag (111) reflections. As shown in Figure 2a,b, after 15 min at 170 °C, the ($22\bar{2}$) peak for Ag-TCNQF$_4$ NWs starts to appear, while the intensity of the Ag(111) peak decreases. This indicates that the Ag-TCNQF$_4$ NWs are growing, while the Ag film is being consumed because of the reaction with the TCNQF$_4$ vapor. After 150 min, the Ag(111) peak completely disappears, and correspondingly the intensity of the ($22\bar{2}$) Ag-TCNQF$_4$ peak stabilizes at a constant value, indicating that the NW growth is completed due to complete consumption of the Ag film. The complete consumption of the Ag layer was confirmed by SEM imaging. Similar real-time XRD measurements for the other three temperatures are presented in Supporting Information Figure S2. Figure 3 shows a summary of the growth kinetics measured for four growth temperatures obtained by integrating the same ($22\bar{2}$) peak of Ag-TCNQF$_4$ (representing the growth of the NWs) and the Ag(111) peak (tracking the consumption of the Ag metal). Fits to the experimental plots were calculated using the Avrami model.[38] This kinetic model considers a reaction of the additive type between the reactants, where the product phase is growing from randomly distributed nuclei within a reactant phase.[39,40] Analysis of solid−vapor reaction data using the Avrami model is commonly used for preliminary identification of the growth rate laws.[41,42] The Avrami exponent (n), usually related to the geometry of the transformation, is believed to give some indication of the mechanism of growth,
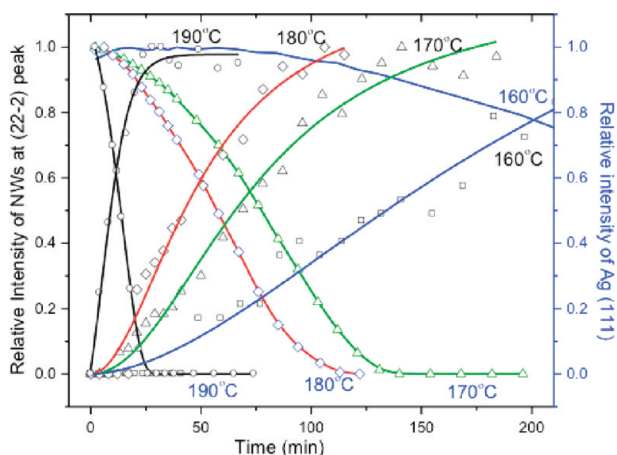
Figure 3. Normalized integral intensities from the real-time XRD of Ag-TCNQF$_4$ nanowire growth from Ag metal at four different temperatures (shown), along with fits from an Avrami model. Growth kinetics of the nanowires is inferred from the rise in the Ag-TCNQF$_4$ (22$\bar{2}$) reflection and consumption of Ag metal is inferred from the loss in Ag(111) reflection.

in particular the balance of the rates of nucleation versus crystal growth. The original derivation of the general relation by Avrami included three limiting cases where $3 \leq n \leq 4$ for three-dimensional growth, $2 \leq n \leq 3$ for two-dimensional growth, and $0 \leq n \leq 2$ for linear or one-dimensional growth. The Avrami exponent is known to vary between 0.5 and 1.5 in the case of one-dimensional, diffusion-controlled reactions. The value of n is close to 0.5 if the nucleation is instantaneous, and close to 1.5 if the nucleation is finite and constant throughout the reaction.[41] For our experimental data, the estimated Avrami exponents and kinetics constants (k) are summarized in Table 1. The n values over the entire temperature range (160−190

Table 1. Estimated Rate Constants (k) and Exponents (n) for the Ag-TCNQF$_4$ Nanowire Growth

temperature [°C]	Avrami model parameters	
	n	$k \times 10^{-3}$ [min^{-1}]
160	1.70	6.4
170	1.58	12.3
180	1.52	19.4
190	1.10	83.2

°C) lie within the range 1.1−1.7. These values are close to the higher limiting value of 1.5 that corresponds to the case of one-dimensional, diffusion-controlled reactions. This indicates that the NW growth is controlled largely by the diffusion of reactive species or crystal growth itself at the sites. The growth rate strongly increases with temperature. An Arrhenius plot of the growth rate data yielded an activation energy of 20.3 kJ/mol (Supporting Information Figure S3). Likewise to NWs grown from Ag films, based on the results of the Avrami model analysis, we demonstrated that the growth of Ag-TCNQF$_4$ NWs from Ag/Si films and Cu-TCNQF$_4$ NWs from Cu films exhibit the same growth rate behavior, indicating a one-dimensional diffusion-controlled mechanism (Supporting Information Figure S5).

To understand the NW growth mechanism, we investigate how the organic molecules and metal are fed to the growing wire. Here, we propose the growth process for Ag-TCNQF$_4$

NWs shown in Figure 4. First, TCNQF$_4$ molecules in the vapor become adsorbed on the Ag surface (Figure 4a). TCNQF$_4$ is
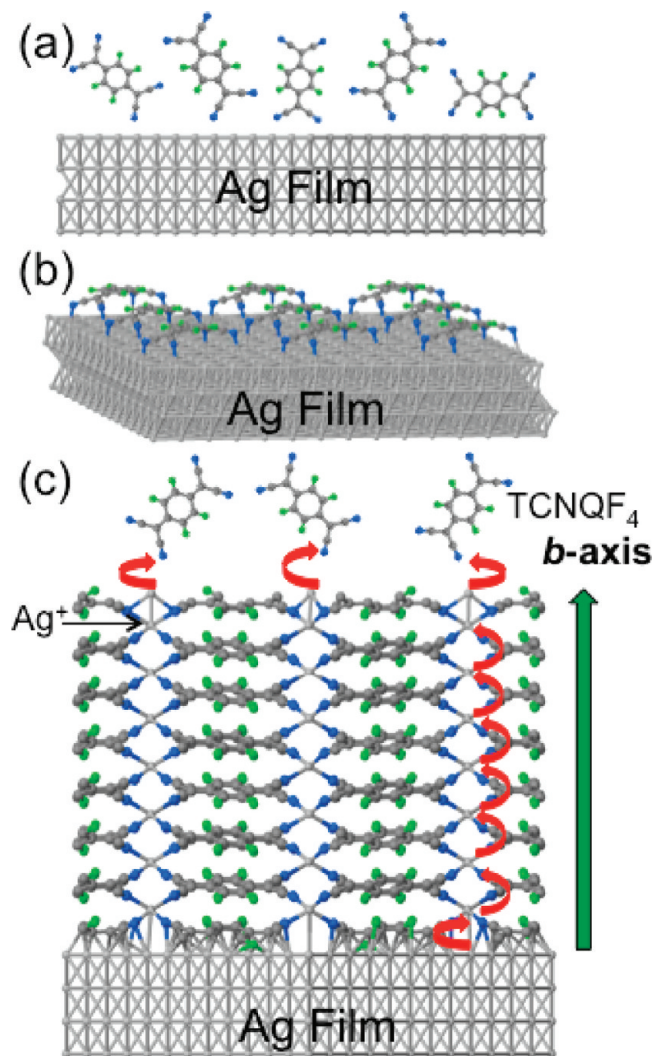
Figure 4. The ionic diffusion tip growth process. (a) TCNQF$_4$ molecules in the vapor become adsorbed on the Ag surface; (b) an electron is extracted from Ag to form a TCNQF$_4^-$ ion. Ag$^+$ is then extracted from the metal film to form Ag-TCNQF$_4$ by chemical reaction. (c) The Ag ions are coordinated to four TCNQF$_4^-$ ions and face-to-face stacking of these molecules forms parallel, periodic 1D channels for Ag$^+$ diffusion. Silver vacancies $\square_{Ag}$ diffuse through the Ag-TCNQF$_4$ layer and undergo Ag ion-exchange with that in the Ag-TCNQF$_4$ complex along the growth direction, then migrate on the top of the NW to react with TCNQF$_4$ vapor to maintain the Ag-TCNQF$_4$ NW growth. (Blue, N; gray, C; green, F; light gray, Ag).

one of the strongest organic electron acceptors with an electron affinity of 5.24 eV.[43] This value is higher than the work function of the Ag (4.26 eV) surface, so it is energetically favorable for an electron to be extracted from the metal to form a TCNQF$_4^-$ ion (Figure 4b). Ag$^+$ is then extracted from the metal film to form the AgTCNQF$_4$ by chemical reaction. Additional TCNQF$_4$ molecules arrive to react with the topmost Ag atom, forming the first Ag-TCNQF$_4$ layer (Figure 4c). In the absence of Ag$^+$ an ionic vacancy (denoted $\square_{Ag}$) is formed, which subsequently diffuses in Ag-TCNQF$_4$ to reach the silver film. As in the first layer formed, it is energetically favorable for Ag$^+$ ions from adjacent layers to replace the ionic vacancy to
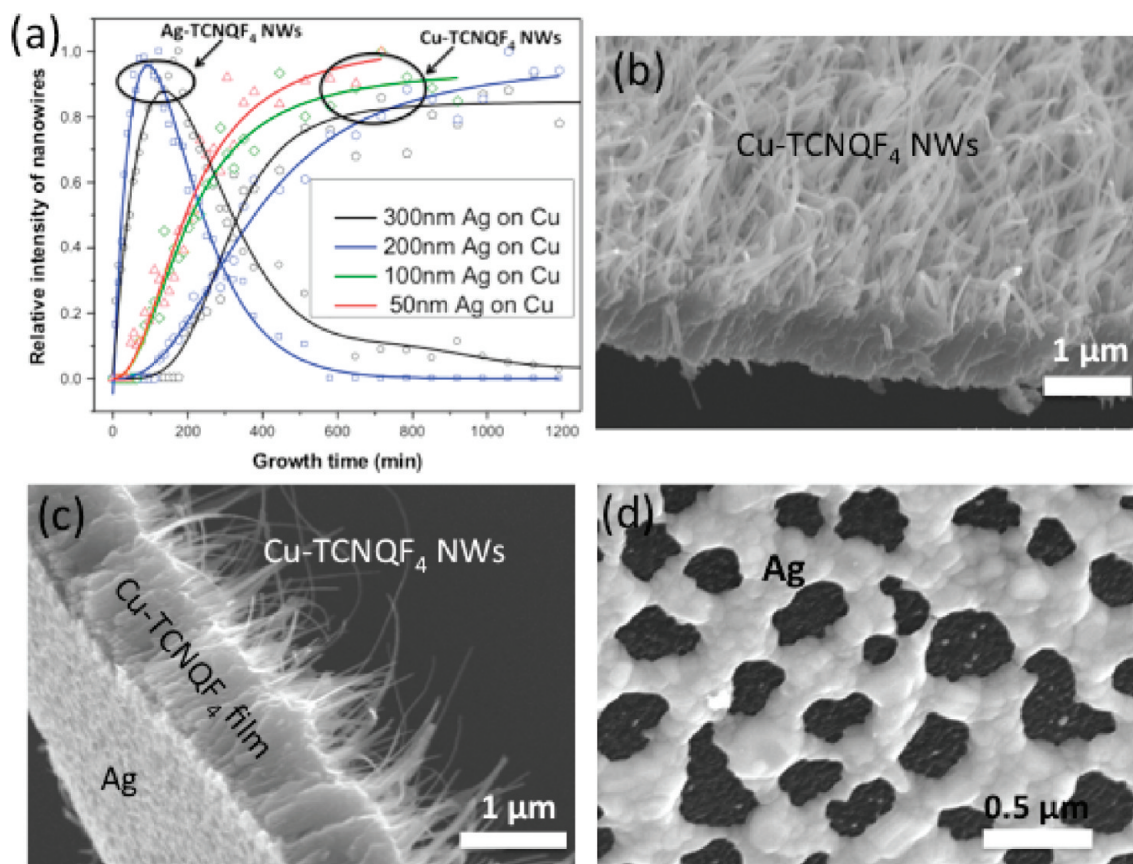
Figure 5. (a) Normalized integral intensities from the real-time XRD of organic NWs growth from various thickness Ag film on 50-nm Cu film at 170 °C, along with fits from an Avrami model. The peak of Ag-TCNQF$_4$ NWs at 15.5° and the peak position of Cu-TCNQF$_4$ NWs at 16.8° are selected as the signature peak to detect NWs growth. When the Ag thickness was less than 200 nm, only the Cu-TCNQF$_4$ NWs were formed (red and green); when the Ag thickness was greater than 200 nm, the intermediate Ag-TCNQF$_4$ forms first and then is changed to Cu-TCNQF$_4$ (dark and blue). (b) SEM image of organic NWs grown from Ag/Cu films; (c) side view of the NWs grown from Ag/Cu film showing the underlying Cu-TCNQF$_4$ layer and the left silver. (d) The backside of NW array showing clearly the copper is consumed completely while the silver remained virtually unchanged after the NWs grown.

form a complete AgTCNQF$_4$ layer. This process is repeated layer by layer, resulting in a migration of Ag ions from the metal surface to the nanowire tip (or conversely, counterpropagating vacancies from the tip to the metal) (see Figure 4c). The Ag ions in the existing structure are coordinated to four TCNQF$_4^-$ ions and face-to-face stacking of these coordinated molecules (determined from previous HRTEM characterization)[18] forms parallel, periodic 1D channels for Ag$^+$ diffusion (as on the topmost layer). This efficient stacking structure can make the Ag ion diffusion and exchange with that in the Ag-TCNQF$_4$ much faster along the [010] direction,[44] leading to the anisotropic growth and producing the NW morphology. To maintain the Ag-TCNQF$_4$ NW growth, silver vacancies □$_{Ag}$ diffuse through the Ag-TCNQF$_4$ layer and exchange with Ag ions in the Ag- TCNQF$_4$ complex along the growth direction, then migrate on the top of the NW to react with TCNQF$_4$ vapor. Metal ions have been reported to pass through a solid complex crystal with a high diffusion rate during the templated growth of Cu-TCNQ NWs in solution.[44,45] Therefore it is reasonable to postulate that diffusion continues during NW growth until the silver at the base of the NWs is consumed completely and the Ag-TCNQF$_4$ NWs finish growing. This mechanism should present a 1D ion diffusion-controlled reaction with a constant nucleation and growth process, consistent with the in situ XRD experimental results and

Avrami model fit to the Ag-TCNQF$_4$ NW growth rate data. As the NWs grow longer and longer, the metal ion supply decreases below that necessary to sustain uniform NW growth, resulting in the formation of a sharp tip, consistent with the experimental observations. However, as the temperature increases, the atomic diffusion rate of Ag increases, providing a sufficient amount of metal ions at the NW tip for uniform growth. These observations further support the proposed tip-growth VSCR ion diffusion-controlled growth mechanism.

Ion-diffusion driven growth mechanisms have been concluded before for inorganic NWs.[46,47] Also, Ag ion diffusion accompanied by ion exchange in Ag-TCNQ films has been reported.[48] Moreover, a vapor—liquid—solid (VLS) model was proposed by Ye et al. to explain the growth mechanism of Ag-TCNQ NWs in the vapor—solid chemical reaction process;[49] however, it is impossible to form liquid Ag at only 170 °C. Our observation of the existence of the Ag-TCNQF$_4$ buffer layer between the Ag-TCNQF$_4$ NWs and the substrate (see Figure 1a) also rules out the possibility of VLS growth, and instead supports an internal ion diffusion model. Our proposed growth mechanism for Ag-TCNQF$_4$ nanowires should apply to the growth of nanowires from other organic acceptors that form charge transfer complexes with metals that have crystalline structures with periodic channels that facilitate metal-ion diffusion, including TCNQ, TCNE, and DCNQI. However,
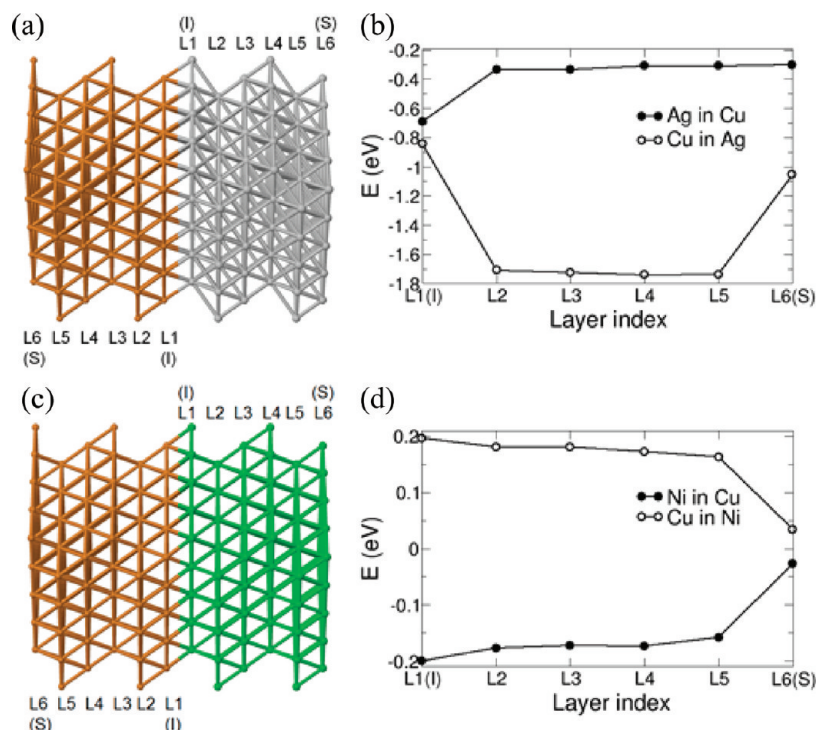
Figure 6. The total energies for doped layer systems of Ag/Cu layers (a and b) or Ni/Cu layers (c and d) in terms of the location of the dopant, where the film consist of 5 × 5 fcc-(111) surfaces of 6 monolayers (ML) and each layer (L) is labeled from L1 to L6, where L1 of each film is the interface (I) layer and L6 represent layers on surfaces (S). We substitutionally doped Cu (Ag) films by Ag (Cu) atoms, and Cu (Ni) films by Ni (Cu) atoms, and calculated changes in total energies with respect to the nondoped structures using Sutton−Chen many-body potential, indicating that it is energetically favorable for Cu and Ag to intermix, but unfavorable to move Cu atoms through the Ni film. (brown balls, gray balls, and green balls for Cu, Ag, and Ni atoms, respectively).

incorporation of metals will alter the electronegativity of these acceptors which may impact the crystal structure and phase stability in these systems.

To check the postulated ion diffusion growth mechanism, another in situ X-ray diffraction experiment was designed to detect long-range metal ion transfer through ionic exchange reactions. Experimentally, it has been reported that the Cu can diffuse very fast through Ag films, which was explained by grain boundary diffusion.[50−52] To understand the effects of interdiffusion in these experiments, nanowire growth was performed on substrates containing film layers of Ag of varying thickness on top of 50 nm Cu (Supporting Information Figure S4). With the use of in situ XRD, the kinetics of nanowire growth involving competitive $TCNQF_4$ reactions with Ag and Cu were observed as a function of the Ag film layer thickness (Supporting Information Figure S5−S8). When the Ag thickness was less than 200 nm, only Cu-$TCNQF_4$ NWs were formed, as shown in Figure 5. In these cases, in situ XRD and postgrowth SEM show that the copper is consumed completely while the silver remained virtually unchanged. The XRD silver peak intensity actually increases a small amount due to preferred grain growth of the Ag film caused by the interdiffusion of the Cu atoms (Supporting Information Figure S7).[53] When the Ag thickness was greater than 200 nm, the in situ XRD showed an initial drop in Ag peak intensity and rise in Ag-$TCNQF_4$ intensity during which time a constant Cu intensity was maintained, indicating an initial reaction between the Ag and $TCNQF_4$. However, with increasing growth time, the Ag peak stopped decreasing and began to increase while the Cu peak began to decline. Meanwhile, the Ag-$TCNQF_4$ NW peak decreases and the Cu-$TCNQF_4$ peak increases (Support-

ing Information Figure S8). This indicates that intermediate Ag-$TCNQF_4$ forms first and then is changed to Cu-$TCNQF_4$.

To understand the mechanism by which Cu might replace Ag in Ag-$TCNQF_4$ nanowires, we performed atomistic modeling calculations for comparison with our experimental findings. Figure 6 presents the total energies for doped layer systems consisting of Ag and Cu in terms of the location of the dopant. The calculations show that it is energetically favorable for Cu and Ag to intermix. For example, there is total energy gain of 0.84 eV when a Cu atom replaces a Ag atom at the interface (L1, I), and another 0.9 eV is gained when the Cu moves to the second layer of the Ag from the interface (L2). Cu motion through Ag layers L3, L4, and L5 is slightly energetically favorable until the surface (L6, S) is encountered, where ∼0.8 eV is required to replace a surface Ag atom. Our ab initio density functional (DFT) calculations show that copper has a significantly stronger chemical binding energy to $TCNQF_4^-$ ions in comparison to silver (the total binding energy is ∼3.0 eV for Ag-$TCNQF_4$ and ∼4.0 eV for Cu-$TCNQF_4$, for the optimized configurations see Figure 7).[54] So if Ag-$TCNQF_4$ molecules were present at the Ag surface, the ∼1.0 eV difference in binding energies between Ag-$TCNQF_4$ and Cu-$TCNQF_4$ would compensate for this surface barrier, and explain the replacement of Ag-$TCNQF_4$ by Cu-$TCNQF_4$ in the experiments. On the other hand, for Ag diffusion through Cu, there are several barriers after the initial energy gain of 0.69 eV for creating a Ag-dopant on the Cu film at the interface. Moving to position L2 requires ∼0.4 eV, and moving to each level costs energy, culminating in a final ∼1 eV barrier to replace Cu-$TCNQF_4$ with Ag-$TCNQF_4$. Therefore, the calculations support the experimental observations that show
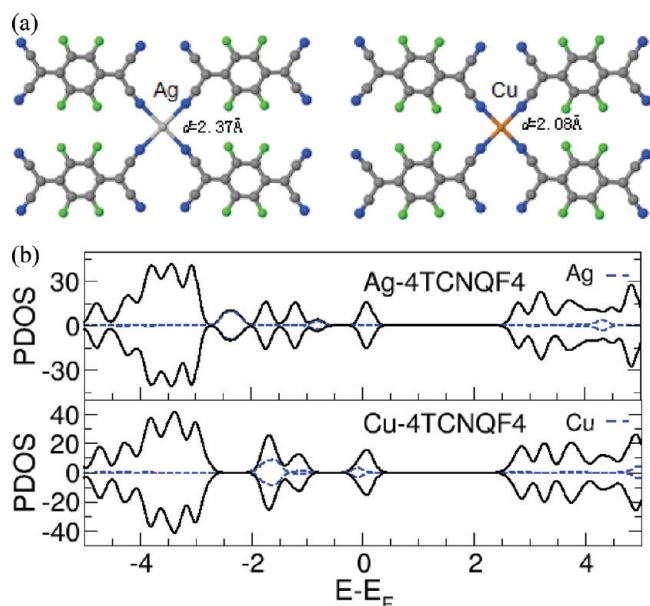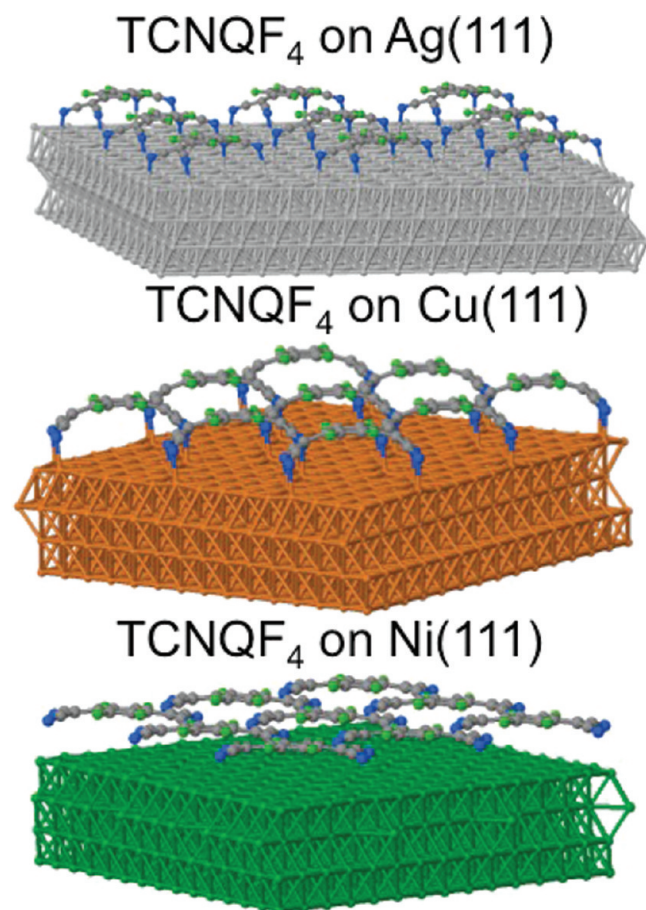
Figure 7. (a) The optimized structures of metal (M)-incorporated $TCNQF_4$ (M = Ag and Cu) show that Cu has a shorter bond length with $TCNQF_4^-$ ions in comparison to silver. (b) Electronic projected density of states (PDOS) of those structures are calculated with respect to the Fermi levels (E_F). The positive and negative values of DOS correspond to spin-up and spin-down components, for each. The black solid lines are contributions from total structures and the dotted-blue lines are from metal atoms. The strong electronic contributions of Cu d-orbitals near the Fermi level help to form a stronger chemical bonding (by ~1 eV) with $TCNQF_4^-$ in comparison to silver.

rapid diffusion of Cu through Ag to replace Ag-$TCNQF_4$ with Cu-$TCNQF_4$.

The stronger binding between $TCNQF_4$ and Cu versus Ag is illustrated in Figure 7a, which presents the optimized structures and a shorter bond length (2.08 vs 2.37 Å) for Cu- versus Ag-$TCNQF_4$. Figure 7b shows the electronic projected density of states (PDOS) with respect to the Fermi levels (E_F) for these two complexes. The black solid lines are contributions from the total structures while the dotted-blue lines are the isolated contributions from the metal atoms, where the positive and negative values correspond to spin-up and spin-down components, respectively. For both cases, there are finite states at the Fermi level indicating their metallic behavior and no net-spins as both up and down spins have peaks at exact same locations. Near the Fermi level there is no contribution from Ag, however, there is a noticeable contribution from Cu (d-orbitals). Therefore we conclude that the strong electronic contributions of Cu d-orbitals near the Fermi level helps form a stronger molecular binding.

To probe the selectivity of metals for an organic reactant and further pinpoint the ion-diffusion growth mechanism of organic NWs, we studied the selective growth of various metals with $TCNQF_4$ molecules. A 50-nm-thick Ni film was deposited on top of a 50-nm Cu film on silicon substrate and attempted VSCR growth at 170 °C. In situ XRD and postgrowth SEM imaging found that nothing grew on the Ni film surface after 20 h (Supporting Information Figure S9). To understand these experimental results, we computationally studied the inter-action between $TCNQF_4$ molecules and Ni(111), Ag(111), and Cu(111) metal films. All the molecules and only the surface layers of the films were fully relaxed during optimization

processes. The optimized configurations are presented in Figure 8. We found significant differences between the

Figure 8. Optimized structures of $TCNQF_4$ molecules on fcc (111) Ag, Cu, and Ni films. The molecules and the top two layers of the films were fully relaxed during the optimization processes. They are strongly bent on the Cu film and slightly bent on the Ag film, while no noticeable changes are observed on Ni, indicating that the molecular interaction is strongest on Cu, weaker on Ag, and negligible on Ni.

optimized configurations. The molecules undergo no noticeable structural changes on Ni(111) and there is no chemical bonding between the molecule and the metal film. On the other hand, the molecules strongly interact with the Ag(111) and Cu(111) surfaces, inducing a strong distortion of their structures. The $TCNQF_4$ adsorption energy is 0.4 eV higher on Cu than that on Ag, resulting in the much stronger distortion of the molecules on Cu than on Ag. The interactions are mediated through the charge transfer mechanism. We calculated changes in total charge densities upon bringing different metal films and $TCNQF_4$ molecules together. Results using the PBE functional show the partial charge transfer of 0.93 e from Ag to $TCNQF_4$, 0.70 e from Cu to $TCNQF_4$, and a significantly smaller (≈0.20 e) from Ni to $TCNQF_4$. We conclude that this weak interaction between the $TCNQF_4$ molecules and the Ni films is responsible for the observed lack of nucleation and growth of Ni-$TCNQF_4$ NWs.

Moreover, unlike the Ag/Cu growth experiment, the Cu underlayer did not diffuse through the Ni overlayer to grow Cu-$TCNQF_4$ NWs. As shown in Figure 6c,d, Cu is not predicted to diffuse through Ni. The energy cost to create a substitutionally

doped Cu at the interface between the Ni and Cu films is ∼0.2 eV, and this energy barrier slightly decreases layer by layer into the Ni film, approaching 0.04 eV at the surface. Thus it is energetically unfavorable to move Cu atoms through the Ni film via substitutional doping.

To test the prediction that Ni might serve as a blocking layer for Cu diffusion, we again deposited Cu as a base layer and Ag as the top layer, but with an interlayer of Ni. In contrast to the Ag/Cu growth experiment, only Ag-TCNQF$_4$ NWs were formed (Supporting Information Figure S10). Copper was unable to replace the Ag$^+$ ions in the TCNQF$_4^-$ lattice because it was unable to diffuse through the Ni film. Also, diffusion in Ni grain boundaries is known to be limited at lower temperatures.[55]

Therefore, the metal layer sequence can have a very large effect in controlling the growth of organic nanowires. Note that although Ni serves as a blocking layer for Cu, our predictions in Figure 6 show that it is energetically favorable for Ni to dope all the layers of Cu. The amount of energy gain through doping is highest at the interface layer (∼0.2 eV) and the lowest on the surface (∼0.03 eV). This behavior can be explained by the high cohesive energy of Ni (4.44 eV) compared to Cu (3.39 eV), resulting in an energy gain when Ni is introduced into Cu, but an energy penalty when doping Cu into Ni.

In summary, our calculations provide an energetic pathway to explain the in situ XRD measurements and growth results that Cu can rapidly diffuse through Ag and replace Ag ions in Ag-TCNQF$_4$, but Cu diffusion is blocked by a Ni interlayer. Understanding these atomistic interactions is very useful for designing processing approaches to integrate organic nanowires in device fabrication, as previously demonstrated.[18] Through understanding and control over the kinetics and pathways for metal ion diffusion and vapor-solid reactions, there is great potential to synthesize novel nanoscale organic axial/coaxial building blocks for ordered heterojunction OPVs.

CONCLUSION

In summary, the reaction pathway and kinetics of metal-TCNQF$_4$ NW growth from TCNQF$_4$ vapor and metal films via VSCR method were investigated using time-resolved in situ X-ray diffraction. The kinetics analysis using a modified Avrami model indicates that the formation of organic nanowires by VSCR follows a 1D ion diffusion-controlled tip-growth mechanism. Metal ions from a metal thin film diffuse along the NW to the tip to react with small molecules to produce uniform and aligned NWs. Deeper insight into the selective reaction between the organic vapor and metals in the deterministic growth of VSCR process is gained from the in situ XRD and atomistic calculations. Experimental data and theoretical calculations indicate that the selectivity of NW growth depends on the interactions between TCNQF$_4$ molecules and metals which are mediated through the charge transfer mechanism. Furthermore, a significantly stronger chemical bonding of TCNQF$_4$ and Cu induced from the strong electronic contributions of Cu d-orbitals can explain the ionic exchange reactions whereby Ag ions in Ag-TCNQF$_4$ are replaced by Cu once they are available to form Cu-TCNQF$_4$ nanowires. This understanding of the kinetics, diffusion, and selective chemical reactions inherent in organic nanowire growth by VSCR is essential to enable efforts to construct novel organic nanostructures consisting of p/n junctions in axial and coaxial nanowires for organic photovoltaic and other electronic devices.

ASSOCIATED CONTENT

S Supporting Information

The detailed in situ XRD scans during temperature-ramp growth of Ag-TCNQF$_4$ nanowires and the metal selectivity growth of organic nanowires. This material is available free of charge via the Internet at http://pubs.acs.org.

AUTHOR INFORMATION

Corresponding Author

xiaok@ornl.gov; geohegandb@ornl.gov

Notes

The authors declare no competing financial interest.

ACKNOWLEDGMENTS

REFERENCES

(1) Zang, L.; Che, Y. K.; Moore, J. S. *Acc. Chem. Res.* **2008**, *41*, 1596.
(2) Briseno, A. L.; Mannsfeld, S. C. B.; Jenekhe, S. A.; Bao, Z.; Xia, Y. *Mater. Today* **2008**, *11*, 38.
(3) Lu, G.; Li, L.; Yang, X. *Small* **2008**, *4*, 601.
(4) Palmer, L. C.; Stupp, S. I. *Acc. Chem. Res.* **2008**, *41*, 1674.
(5) Yang, F.; Shtein, M.; Forrest, S. R. *Nat. Mater.* **2005**, *4*, 37.
(6) Xiao, K.; Li, R.; Tao, J.; Payzant, E. A.; Ivanov, I. N.; Puretzky, A. A.; Hu, W.; Geohegan, D. B. *Adv. Funct. Mater.* **2009**, *19*, 3776.
(7) Karak, S.; Ray, S. K.; Dhar, A. *J. Phys. D: Appl. Phys.* **2010**, *43*, 245101.
(8) Zhang, Y.; Dong, H.; Tang, Q.; Ferdous, S.; Liu, F.; Mannsfeld, S. C. B.; Hu, W.; Briseno, A. L. *J. Am. Chem. Soc.* **2010**, *132*, 11580.
(9) Xiao, K.; Tao, J.; Pan, Z.; Puretzky, A. A.; Ivanov, I. N.; Pennycook, S. J.; Geohegan, D. B. *Angew. Chem., Int. Ed.* **2007**, *46*, 2650.
(10) Liu, H.; Zhao, Q.; Liu, Y. L.; Liu, Y.; Lu, F.; Zhuang, J.; Wang, S.; Jiang, L.; Zhu, D. B. *J. Am. Chem. Soc.* **2005**, *127*, 1120.
(11) Ye, C.; Cao, G.; Fang, F.; Xu, H.; Xing, X.; Sun, D.; Chen, G. *Micro* **2005**, *36*, 461.
(12) Xiao, K.; Tao, J.; Puretzky, A. A.; Ivanov, I. N.; Retterer, S. T.; Pennycook, S. J.; Geohegan, D. B. *Adv. Funct. Mater.* **2008**, *18*, 3043.
(13) Liu, H.; Wu, X.; Chi, L.; Zhong, D.; Zhao, Q.; Li, Y.; Yu, D.; Fuchs, H.; Zhu, D. *J. Phys. Chem. C* **2008**, *112*, 17625.
(14) Liu, Y. L.; Liu, H. X.; Du, D. Y.; Ji, Z. Y.; Wang, C. S.; Tang, Q. X.; Liu, M.; Hu, W. P.; Liu, Y. Q.; Zhu, D. B. *J. Am. Chem. Soc.* **2006**, *128*, 12917.
(15) Bong, D. B.; Clark, T. D.; Granja, J. R.; Ghadiri, M. R. *Angew. Chem., Int. Ed.* **2001**, *40*, 988.
(16) Zhao, C.; MacFarlane, D. R.; Bond, A. M. *J. Am. Chem. Soc.* **2009**, *131*, 16195.
(17) Tsivion, D.; Schvartzman, M.; Popovitz, R.; von Huth, P.; Joselevich, E. *Science* **2011**, *333*, 1003.
(18) Xiao, K.; Rondinone, A. J.; Puretzky, A. A.; Ivanov, I. N.; Retterer, S. T.; Geohegan, D. B. *Chem. Mater.* **2009**, *21*, 4275.
(19) Ouyang, C. B.; Guo, Y. B.; Liu, H.; Zhao, Y.; Li, G.; Li, Y.; Song, Y.; Li, Y. *J. Phys. Chem. C* **2009**, *113*, 7044.
(20) Xiao, K.; Ivanov, I. N.; Puretzky, A. A.; Liu, Z.; Geohegan, D. B. *Adv. Mater.* **2006**, *18*, 2184.
(21) Di, C.; Yu, G.; Liu, Y.; Xu, X.; Wei, D.; Song, Y.; Sun, Y.; Wang, Y.; Zhu, D.; Liu, J.; Liu, X.; Wu, D. *J. Am. Chem. Soc.* **2006**, *128*, 16418.
(22) Millange, F.; Medina, M. I.; Guillou, N.; Ferey, G.; Golden, K. M.; Walton, R. I. *Angew. Chem., Int. Ed.* **2010**, *49*, 763.
(23) Cravillon, J.; Schroder, C. A.; Nayuk, R.; Gummel, J.; Huber, K.; Wiebcke, M. *Angew. Chem., Int. Ed.* **2011**, *50*, 8067.

(24) Mi, J.; Jensen, T. N.; Christensen, M.; Tyrsted, C.; Jorgensen, J. E.; Iversen, B. B. *Chem. Mater.* **2010**, *23*, 1158.

(25) Blum, V.; Gehrke, R.; Hanke, F.; Havu, P.; Havu, V.; Ren, X.; Reuter, K.; Scheffler, M. *Comput. Phys. Commun.* **2009**, *180*, 2175.

(26) Ceperley, D. M.; Alder, B. J. *Phys. Rev. Lett.* **1980**, *45*, 566.

(27) Perdew, J. P.; Burke, K.; Ernzerhof, M. *Phys. Rev. Lett.* **1997**, *77*, 3865.

(28) Zhang, Y.; Yang, W. *Phys. Rev. Lett.* **1998**, *80*, 890.

(29) Perdew, J. P.; Wang, Y. *Phys. Rev. B* **1992**, *45*, 13244.

(30) Press, W. K.; Teukolsky, S. A.; Bethe, H. A.; Vetterling, W. T.; Flannery, B. P. *Numerical Recipes*, 3rd ed.; Cambridge University Press: Cambridge, England, 2007.

(31) Kresse, G.; Furthmuller, J. *Phys. Rev. B* **1996**, *54*, 11169.

(32) Monkhorst, H. J.; Pack, J. D. *Phys. Rev. B* **1976**, *13*, 5188.

(33) Sutton, A. P.; Chen, J. *Philos. Mag. Lett* **1990**, *61*, 139.

(34) Rafiitabar, H.; Sutton, A. P. *Phil. Mag. Lett.* **1991**, *63*, 217.

(35) Qi, Y.; Cagin, T.; Kimura, Y.; Goddard, W. A., III. *Phys. Rev. B* **1999**, *59*, 3527.

(36) O'Kane, S. A.; Clerac, R.; Zhao, H.; Ouyang, X.; Galan-Mascaros, J. R.; Heintz, R.; Dunbar, K. R. *J. Solid State Chem.* **2000**, *152*, 159.

(37) Kraus, T. N.; Barrena, E.; Lohmuller, T.; Spatz, J. P.; Dosch, H. *Phys. Chem. Chem. Phys.* **2011**, *13*, 5940.

(38) Avrami, M. *J. Phys. Chem.* **1941**, *9*, 177.

(39) Zhou, Y.; Pienack, N.; Bensch, W.; Patzke, G. R. *Small* **2009**, *5*, 1978.

(40) Choi, S. Y.; Mamak, M.; Speakman, S.; Chopra, N.; Ozin, G. A. *Small* **2005**, *1*, 226.

(41) Kim, W. K.; Payzant, E. A.; Yoon, S.; Anderson, T. J. *J. Cryst. Growth* **2006**, *294*, 231.

(42) Jeon, K. J.; Moon, H. R.; Ruminski, A. M.; Jiang, B.; Kisielowski, C.; Bardhan, R.; Urban, J. J. *Nat. Mater.* **2011**, *10*, 286.

(43) Gao, W. Y.; Kahn, A. *J. Appl. Phys.* **2003**, *94*, 359.

(44) Ji, H.; Hu, J.; Guo, Y.; Song, W.; Wan, L. *Adv. Mater.* **2008**, *20*, 4879.

(45) Duan, H.; Cowan, D. O.; Kruger, J. *J. Electrochem. Soc.* **1993**, *140*, 2807.

(46) Zhang, W.; Yang, S. *Acc. Chem. Res.* **2009**, *42*, 1617.

(47) Liu, X.; Mayer, M. T.; Wang, D. *Angew. Chem., Int. Ed.* **2010**, *49*, 3165.

(48) Liu, P.; Jiang, Y.; Xie, H.; Guo, F.; Li, J. *Jpn. J. Appl. Phys.* **2005**, *44*, L494.

(49) Ye, C.; Cao, G.; Mo, X.; Fang, F.; Xing, X.; Chen, G.; Sun, D. *Chin. Phys. Lett.* **2004**, *21*, 1787.

(50) Pitts, J. R.; Czanderna, A. W.; Thomas, T. M. *J. Vac. Sci. Technol., A* **1986**, *4*, 1671.

(51) Jones, D. A.; Jankowski, A. F.; Davidson, G. A. *Metall. Mater. Trans. A* **1997**, *28A*, 843.

(52) Yildirim, H.; Rahman, T. S. *Phys. Rev. B* **2009**, *80*, 235413.

(53) Zoo, Y.; Han, H.; Alford, T. L. *J. Appl. Phys.* **2007**, *102*, 083548.

(54) We consider metal (M)-incorporated $TCNQF_4$ as building blocks of nanowires. These molecules resemble the symmetry of the M's d-orbital and 4 $TCNQF_4$ molecules are connected by M in the center. Figure 6 shows the fully optimized structures from PBE functional. The distances from metal to the molecules, in particular the bond distances between M and F, are shorter (by 0.3 Å) for Cu than those from Ag; usually, a shorter bond length is an indication of stronger binding. In fact, both metals form very strong chemical bonding to the molecules; the total binding energy is ≈3.0 eV for Ag-4TCNQF$_4$ and ≈4.0 eV for Cu-4TCNQF$_4$, in comparison to the energies of the systems of individual M atoms and noninteracting molecules.

(55) Sheng, J.; Welzel, U.; Mittemeijer, E. J. *Adv. Mater. Res.* **2010**, *89–91*, 503.